

1
2 Combined with the 1960-2012 modelled values, this produces a continuous record
3 of estimated annual runoff for 1871-2012. Average monthly variability in runoff is
4 superimposed on this record using the β_{month} term.

6 | 4.3 Confluence with AS: adjustments to d_w and ice flux

7 While KNS and AS are confluent in model simulations, variability in d_w at the
8 terminus is driven by total runoff values from both catchments. The confluence area
9 of the two glaciers is defined on the model flowline as being 5 km across, lying
10 between 4 km and 9 km from the 2012 terminus position. However, as KNS retreats
11 through ~~its the~~ confluence with AS ~~this will remove~~ the runoff contribution from AS to
12 the terminus is removed, meaning that d_w needs to be scaled to reflect this. Modelled
13 annual runoff totals for each catchment show that KNS and AS respond directly in
14 phase with one another ($r = 0.99$), with KNS accounting for 70.3% (MARv3.2) or
15 74.6% (RACMO2) of total runoff (Van As et al., 2014). To allow for this reduction in
16 runoff as KNS retreats through the confluence, the value of d_w is multiplied by a
17 scale factor, γ , that will have a fixed value for each model run of between, α_2 (a
18 confluence scaling factor) and 1, such that

$$19 \quad d_{wNew} = \gamma d_{wPrev} \quad (4)$$

21
22 Because AS and KNS will at times be partially confluent, the value of γ is also scaled
23 linearly with respect to the relative position of the terminus through the confluence,
24 such that when they are fully confluent $\gamma = 1$, and when fully diffluent $\gamma = \alpha_2$. Values
25 are varied linearly between α_2 and 1 for terminus positions within the confluence
26 according to

$$27 \quad \gamma = \alpha_2 + (1 - \alpha_2) \left(\frac{x_{conf}}{X_{conf}} \right) \quad (5)$$

29
30 | Where x_{conf} ~~is the~~ distance of the terminus through the confluence, and X_{conf} ~~is~~
31 the total flowline distance over which the confluence occurs. Due to uncertainty
32 regarding the precise scaling of runoff to d_w as KNS retreats through its confluence

1 with AS, and other confluence effects, α_2 is used as a tuning parameter within the
2 model.

3 The extra ice flux contribution from AS when confluent with KNS is estimated
4 to be approximately one sixth of that of KNS, based on the contemporary across
5 glacier velocity profiles (Joughin et al., 2010), and terminus widths of AS and KNS.
6 This extra flux is added to the modelled glacier as positive SMB at the confluence of
7 KNS and AS, distributed along the flowline proportionate to the contemporary AS
8 across glacier velocity profile (Lea et al., 2014a).

9

10 | **4.4 Relating submarine melt ~~rate~~ to sea surface temperature**

11 Submarine melt rate (M) has previously been linearly related to deep ocean
12 temperature (DOT) variability using a scaling coefficient (Nick et al., 2013; their
13 equation S2). Using this parameterisation, the highest values of M (expressed in this
14 study in $\text{km}^3 \text{a}^{-1}$) are associated with the highest scaling coefficients. Therefore high
15 scaling factor values would also be linked to the highest inter-annual variability of M .
16 | This study ~~therefore~~ takes a slightly different approach in that (1) M is scaled to sea
17 surface temperature (SST) rather than DOT, for reasons relating to fjord circulation
18 explained above, and (2) we introduce a constant (minimum) baseline M rate, M_{base} ,
19 | which is added to the linear relation ~~to-with~~ SST. We therefore calculate M ($\text{km}^3 \text{a}^{-1}$)
20 according to

21

$$22 \quad M = M_{base} + \alpha_3 T_{year} \quad (6)$$

23

24 Where α_3 is a submarine melt rate scaling coefficient, and T_{year} is the annual average
25 SST. This allows ~~different-multiple~~ minimum background rates M_{base} to be tested for
26 different model runs, with ~~different-various~~ sensitivities of M to changes in SST
27 superimposed upon this, using ~~different-values-of~~ α_3 .

28

29 | **4.5 Model experiments and evaluation**

30 Tuning parameters α_1 , α_2 , α_3 and M_{base} were varied randomly within prescribed limits
31 for a total of 1500 Monte Carlo style model runs. These were defined at the start of
32 each run's spin up period and held constant throughout. The limits for each of the
33 tuning parameters were: (1) α_1 , between 0 and 1.5, (2) α_2 , between 0.3 to 0.8, (3)

1 M_{base} , between 0 to 0.7 km³ a⁻¹, and (4) α_3 , between 0 to 0.3. These ranges of α_1 and
 2 α_2 were chosen to reflect a wide range of potential forcing scenarios, while the
 3 values of M_{base} and α_3 were chosen so total submarine melt rates could potentially
 4 range from 0 km³ a⁻¹ to values that exceed those ~~observed-estimated~~ for other
 5 TWGs in western Greenland (Rignot et al., 2010; Enderlin and Howat, 2013). This
 6 allowed ~~the the feasibility of~~ different potential drivers of the observed terminus
 7 change to be comprehensively assessed. Runs were conducted for the period 1871-
 8 2012, given that this is the period that both atmospheric and oceanic climate records
 9 are available for. The model was initialised at approximately the ASM profile and
 10 terminus position, as defined by the geomorphology, and given the duration of the
 11 spin up period to stabilise for the given forcing scenario. During spin up, d_w was
 12 allowed to freely evolve by up to ± 3 m a⁻¹ to allow the terminus to stabilise at the
 13 ASM, with R_{base} and T_{year} held constant. These were defined as the 1871-1920 runoff
 14 average (3.107 Gt yr⁻¹) and SST average (2.605 °C) respectively. These values were
 15 used for spin up as it is known the ASM was attained at some point within this time
 16 window.

17 Model results were evaluated against their ability to replicate observed
 18 terminus dynamics, where absolute terminus positions are known (i.e. 1921 to 2012).
 19 The period from 1871-1920 therefore effectively becomes a transient spin up period,
 20 where the model is driven using real climate data though terminus position is only
 21 known within a range. The ability of each model run to replicate observed dynamics
 22 was determined using a weighted regression (R^2) calculation, with the weighting of
 23 each terminus observation calculated according to

$$25 \quad w_n = \frac{D_{n+1} - D_{n-1}}{2(D_k - D_1)} \quad \text{for } n = 1, 2, \dots, k \quad (7)$$

26
 27 Where w is the observation weighting in the regression calculation, n is the terminus
 28 observation, k is the total number of terminus observations, and D is the date of the
 29 terminus observation. Each terminus observation is therefore temporally weighted
 30 according to the median length of time elapsed between the terminus observations
 31 that occur before and after observation n . This ensures that the evaluation of model
 32 performance is not biased towards the last ~20 years where there is a comparatively
 33 high density of observations. Model runs were counted as successful where (1) the

1 difference between the modelled and observed 1921 position was <500 m, (2) the
2 weighted $R^2 > 0.85$, and (3) the gradient of the resulting line of regression was >
3 0.85.

4

5 **5. Glacier reconstruction results**

6 The geomorphology shows distinct upper and lower sets of lateral moraines on both
7 sides of the fjord, with fluted moraines occupying the intervening space (Figure 1a).
8 The upper set are associated with the LIA maximum (Lea et al, 2014a), while the
9 lower set were formed during the Akullersuaq Stade. Fridtjof Nansen's (1890)
10 account of the first traverse of Greenland in 1888, includes a drawing from a
11 photograph showing AS and KNS to be confluent, though the terminus position itself
12 is not visible. Although the original image could not be traced or an exact date of
13 acquisition determined, it is likely to have been taken some time near to the
14 publication date of 1890.

15 Maps from 1859, 1860, 1866 and 1885 all show the terminus of KNS to be
16 adjoining Akullersuaq and fully confluent with AS (Kleinschmidt, 1859; Poulsen,
17 1860; Brede, 1866; Rink, 1866; Jensen, 1885). While it is possible that some details
18 on the maps were copied following Kleischmidt (1859), the addition of detail such as
19 lakes on plateaus near to KNS by Jensen (1885) provides confidence that this map
20 faithfully records the contemporary terminus position. There is nothing to suggest
21 that KNS became diffluent from AS at any time from 1859-1885. However, due to a
22 lack of map detail and the Nansen (1890) drawing not including the terminus, these
23 sources cannot be used to provide absolute terminus positions.

24 The earliest images of KNS are from the 1850s and 1903. Both are taken
25 from approximately the same position, with the terminus partially obscured by
26 foreground topography (Weidick et al., 2012). The presence of medial moraines in
27 each image demonstrates that KNS was confluent with AS. Lea et al., (2014a)
28 quantified the terminus position uncertainty for the 1850s photograph using viewshed
29 analysis. Similar analysis has been undertaken for the 1903 image, showing that the
30 uncertainty in terminus position is the same as for the 1850s image (Figure 3). The
31 maximum terminus extents for both images are therefore located behind a headland
32 corresponding to the ASM on the eastern side of the fjord (Figures 1a, 3).

33 It is not currently possible to say from any observational evidence when the
34 ASM was attained ~~from any observational evidence~~, only that it occurred sometime

1 between 1859-1920. The climate anomalies for the period (compared to 1961-1990
 2 baselines) show that air temperature (AT) and SST anomalies were, on average,
 3 antiphased for the period 1871-1903 (Figures 4c, d), though AT and SST anomalies
 4 are in phase (negative/near-baseline) for 1903-1920. Conditions are therefore more
 5 likely to have been conducive for glacier advance during the latter period.

6 Terminus position was mapped directly for the remaining images, providing a
 7 record of 29 terminus positions spanning the period 1921-2012 (Figures 1 and 4).
 8 The first direct terminus observation (1921) shows a slight retreat from the ASM.
 9 Subsequent to this, KNS retreated a total of 9.7 km at a non-uniform rate up to 2012,
 10 interrupted by short periods of readvance (Figures 4a, b). Averaged retreat rates of -
 11 116 m a^{-1} are observed between 1921-1946, before a rapid retreat of 3.9 km within
 12 the 2 year period from 1946-1948 (Figures 1a, 4). Between 1948-1968 KNS
 13 retreated on average by -97 m a^{-1} , before readvancing by $+60 \text{ m a}^{-1}$ up to 1979
 14 (Figure 4b). A terrestrial photograph taken in 1965 with the majority of the terminus
 15 obscured shows the termini of KNS and AS to be fully diffluent.

16 The 1921-1968 period of sustained retreat was accompanied by positive
 17 average AT and SST anomalies (Figures 4c, d). The highest AT anomalies occurred
 18 during the period 1928-1941, though the largest retreat (between 1946-1948)
 19 occurred during a comparatively less extreme period of positive AT and SST (Figure
 20 4).

21 From 1979 to 1987 KNS retreated by -658 m in total (-82 m a^{-1}), before
 22 readvancing by +758 m from 1987-1992 ($+152 \text{ m a}^{-1}$). Using the near complete 20
 23 year annual record of terminus fluctuations from 1992-2012, KNS advanced for 4 out
 24 of 5 years between 1992-1997, followed by retreat in 11 out of 13 years from 1999-
 25 2012 at an average rate of -103 m a^{-1} . The latter included 8 annual retreats of >100
 26 m, with the largest retreats occurring in 2004 (-438 m) and 2005 (-316 m). These
 27 periods of advance and retreat behaviour occurred during periods of in-phase
 28 negative and positive climate anomalies respectively.

29 Where temporal density of observations was high, terminus behaviour that
 30 was antiphased with the prevailing climate anomalies was also observed (i.e.
 31 advancing during positive temperature anomalies, or retreating during negative
 32 temperature anomalies). Examples of this include a retreat of -626 m ~~observed~~ in
 33 1995 ~~during negative~~ when both climate anomalies ~~were negative~~, while ~~two~~ terminus
 34 advances occur in 2008 and 2009 despite markedly positive AT and SST anomalies

(Figure 4). At annual resolution, the magnitude of terminus retreat/advance was also found to be unrelated to the magnitude of either climate anomaly for each particular year.

Based on interpolated terminus positions between observations, terminus widths were consistent at ~3.5 km from 1932-1946, and ~4.2 km from 1968-2012 where terminus change was comparatively slow (Figure 5b). Although fjord depths at the terminus for these periods were more variable, they did not exceed a range of ± 22 m. Fjord width and depth at the terminus displayed two step changes during the retreats between 1921-1932, and 1946-1948 (black lines, Figures 5a-c). During the first of these, both width and depth increased (by ~550 m and 44 m respectively) whereas during the second, width increased but depth decreased (by ~700 m and 146 m respectively). Fjord width and depth at the terminus displayed two step changes during retreat from 1921-2012 (black lines, Figures 5a-c). These occurred during the retreats between 1921-1932, and 1946-1948. Based on interpolated terminus positions between observations, terminus widths were consistent at ~3.5 km from 1932-1946, and ~4.2 km from 1968-2012 where terminus change was comparatively slow (Figure 5b). Fjord depths at the terminus for these periods were more variable, they did not exceed a range of ± 22 m. This is in contrast to the rapid changes in fjord depth at the terminus of 44 m and 146 m occurring between 1921-1928 and 1946-1948 respectively (Figure 5c).

Formatted: Font: Not Italic

6. Model results

From a total of 1500 model runs conducted, 29 runs (1.9%) successfully replicated the observed dynamics of KNS according to the criteria outlined above (Figure 5). Following the initiation of climate forcing in 1871 (Figures 5d, 5e), the results of each run are highly comparable up to 1884, with little modelled terminus change observed. Following this, for the period 1884 to ~1910, 6 of the 29 runs (21%) show evidence of multi-annual terminus retreats and equivalent readvances of >750 m with periodicities of 2-4 years. A further 7 runs (24%) show evidence of at least one short lived (<5 year) oscillation in terminus position of >750 m between 1884 to 1920. None of these model runs significantly exceed the ASM position, and are thus in agreement with the geomorphological evidence presented, and the position of the 1921 terminus observation.

1 All model runs retreat to the observed 1932~~6~~ position between modelled years
 2 1929-1936, via a single retreat event of ~1 km. Subsequent to this, modelled retreat
 3 to the observed 1946 position is gradual, before the model successfully replicates a
 4 large topographically controlled retreat from the 1946 position. There was varying
 5 success in modelling the exact timing of this retreat (observed between 1946-1948),
 6 with the model ensemble predicting it to occur anywhere between 1943-1962. The
 7 position where the modelled terminus restabilises following the retreat through the
 8 AS confluence is generally too far advanced by ~1 km compared to the position
 9 following the 1946-1948 retreat. All model runs then go on to over-predict terminus
 10 extent for the 1968 observation by between 0.35 to 1.59 km.

11 Though no model runs exactly match the precise inter-annual terminus
 12 fluctuations from 1968-2012, they do capture the general multi-annual to decadal
 13 pattern of retreat observed. This is characterised by general terminus stability within
 14 a range of ± 500 m for the period 1968 to ~1999, before the terminus begins to
 15 retreat ~2 km towards the 2012 position. All of the successful model runs identified
 16 predict KNS to be in a more retreated position in 2012 than observed by a range of
 17 0.32 to 5.04 km.

18 Where a significant difference between observed and modelled terminus
 19 positions has occurred by the end of the model run in 2012, the divergence begins in
 20 2010 at the earliest. This coincides with a widening of the modelled fjord associated
 21 with the uncertainty in fjord topography upstream of the contemporary terminus
 22 (Figure 5b).

23 The distributions of tuning parameters for successful runs are shown in Figure
 24 6, with the distribution of all histograms shown to be non-normal. Submarine melting
 25 related tuning parameters, α_3 , and M_{base} , tended towards the mid to lower ends of
 26 the ranges tested (Figures 6c, 6d). Values of α_3 peak between 0.075 to 0.1, though
 27 there is no clearly defined peak in the distribution of M_{base} values.

28 In contrast, none of the d_w related tuning parameters (α_1 and α_2) approach 0
 29 (Figures 6a, 6b), with the lowest values being 0.412 and 0.389 respectively.
 30 Construction of a correlation matrix comparing all tuning parameter values for all
 31 successful runs also demonstrates a significant inverse relationship between the
 32 value of α_1 , and the AS confluence parameter, α_2 ($r = -0.92$). While other significant
 33 correlations are observed (Table 3), these are not of sufficient strength to allow
 34 confident conclusions to be drawn.

7. Discussion

7.1 Observed terminus behaviour

From 1903 to 2012 AT and SST anomalies covaried, with the terminus generally undergoing retreat during periods of positive anomalies and advancing/stabilising when near/below baseline climate (Figure 4). Exceptions to this in-phase behaviour were only identified for the period 1992-2012, where a higher temporal density of terminus observations exists. However, by averaging annual observations over periods of sustained negative (1987-1997) and positive (1998-2012) climate anomalies, the terminus responds in phase with the climate anomalies. This demonstrates the risks of using short datasets (2-5 years) to determine how a TWG is responding to climate forcing, highlighting the inherent noisiness, potential importance of antecedence, and the non-linearity of TWG response to climate.

A notable caveat to this occurs where significant topographically controlled glacier retreats occur (i.e. those driven by changes in fjord width and/or depth), such as the one occurring between 1946-1948. These events could potentially skew annually averaged terminus change rates when attempting to characterise terminus response to climate forcing. The relative importance of this will be entirely dependent on the magnitude of individual events, and most significant where there is potential for multi-kilometre topographically controlled retreat. For example, if the 1946-1948 retreat event was not temporally well constrained, it could have significantly biased the terminus change rate values between 1936-1968 (Figure 4b).

The large terminus retreat between 1946-1948 retreat is accompanied by large changes to both fjord width widens and depth shallows at the terminus (Figures 5a-c). A step change in width and depth is also observed between while the 1921-1932 retreat is associated with a fjord widening and deepening (Figures 5a-c). though there are insufficient observations to establish whether this occurred as rapidly at the 1946-1948 retreat. The 1946-1948 retreat is therefore likely to have been controlled by changes in lateral topography rather than basal topography, whereas the 1921-1932 retreat (if it occurred rapidly, e.g. in 1-2 years) likely resulted from a combination of both. In the intervening periods between these >1 km retreats, both fjord width and depth at the terminus remained largely consistent (Figures 5b,c). While kilometre scale, rapid retreat of KNS is likely due to

Formatted: Font: Not Italic

~~a combination of , indicating the necessity for termini to retreat into fjord widenings or overdeepenings (e.g. Mercer, 1961; Carr et al., 2013; 2014; Porter et al., 2014) the 1946-1948 retreat helps to demonstrate that to destabilising changes in one aspect of fjord topography can dominate stabilising changes in the other, until a new equilibrium is reached instigate rapid retreat (e.g. Mercer, 1961; Carr et al., 2013; 2014; Porter et al., 2014), before the terminus achieves a new stable configuration.~~

Formatted: Indent: First line: 1.27 cm

Since TWGs exhibit varying degrees of non-linearity in response to climate forcing, the identification of where and when these rapid multi-kilometre retreat events occur is crucial for interpreting the causes of terminus fluctuations. Where comparatively smaller (i.e. <500 m) climatically anti-phased advance/retreat events occur, their effect on average terminus change rates can be mitigated by averaging change over timescales up to, or greater than a decade. For example, extending the 1992-1997 average (51 m a⁻¹ retreat) to cover the period 1987-1997 (91 m a⁻¹ advance) provides a more representative impression of multi-annual terminus behaviour, since 5 out of the 6 observations available show terminus advance.

~~Where observations are separated by >1 year, interpreting the absolute values of terminus change rates values should therefore be done with caution, and in most cases these values will be more representative of the average direction (i.e. advance/retreat), rather than the average distance of terminus change rather than the absolute magnitude of annual change.~~

~~The large terminus retreat between 1946-1948 is accompanied by large changes to both fjord width and depth at the terminus (Figures 5a-c). A step change in width and depth is also observed between 1921-1928, though there are insufficient observations to establish whether this occurred as rapidly at the 1946-1948 retreat. In the intervening periods between these retreats, both fjord width and depth at the terminus remained consistent, indicating the necessity for termini to retreat into fjord widenings or overdeepenings to instigate rapid retreat (e.g. Mercer, 1961; Carr et al., 2013; 2014; Porter et al., 2014), before the terminus achieves a new stable configuration.~~

Taking into account uncertainties due to topographic controls on terminus stability, observations of terminus change over a period of several years are more likely to allow a more accurate evaluation provide a better indication of a TWG's response to climate forcings. However, for this study, deconvolving the relative

1 importance of AT versus SST in driving terminus change is difficult using
2 observations alone, given that both climate drivers vary in phase for 1903-present. It
3 could potentially be argued that AT is the primary driver of change, since the 33 year
4 period of positive anomaly SST from 1871-1903 had relatively little impact on the
5 terminus stability of KNS. However, a narrow, and relatively shallow fjord geometry
6 in this region could also have been a significant factor in stabilising the terminus
7 during this time (Figure 3c). Arguably this becomes less likely when it is considered
8 that while SST was similar for the period 1921-1948, positive AT allowed KNS to
9 retreat through the same section of fjord and through its confluence with AS within
10 26 ± 1 years (Figure 4). However, given the lack of certainty in terminus position
11 between 1871-1920, it is not possible to robustly verify these arguments.

12

13 **7.2 Implications of modelling**

14 The observed terminus behaviour of KNS from 1921-2012 was successfully
15 replicated by 29 of 1500 model runs using surface runoff and SST records as drivers
16 of terminus change. This demonstrates that the parameterisations used to scale
17 these climate records to d_w and M respectively can successfully be used to simulate
18 the observed pattern of ~~behaviour of a~~ tidewater glacier behaviour over centennial
19 timescales. Where the observational record is of sufficient detail to resolve inter-
20 annual terminus fluctuations (1992-2012), the model does not replicate these. This is
21 to be expected given (1) the flowband nature of the model and associated depth and
22 width integrations over each grid cell, meaning that fluctuations of terminus
23 configurations such as the creation of calving bays cannot be replicated (e.g. Figure
24 1b), (2) the uncertainty in fjord bathymetry and geometry potentially affecting relative
25 terminus stability, and (3) the use of single terminus observations as notionally
26 definitive indicators of annual terminus change, where the stochastic nature of
27 calving and associated sub-annual terminus fluctuations make any direct one-to-one
28 comparisons of to modelled results ~~to annual resolution observations~~ inappropriate.
29 Valid comparison of model results to observations should therefore only be
30 attempted over multi-annual timescales where terminus dynamics within calving
31 bays, sub-annual calving events and fine scale uncertainties in fjord, and basal
32 topography become comparatively less significant.

33 For successful model runs, the interrelationships between the parameter
34 values that determine d_w and M sensitivity to the climate records also inform the

1 relative importance of changes in atmospheric and oceanic forcing in driving
2 terminus change. The lack of any significant relationship between α_1 and α_3
3 demonstrates that a change in model sensitivity to surface runoff is not offset by any
4 change in model sensitivity to SST (e.g. a higher α_1 would not need to be offset by a
5 lower α_3 for the model run to match observations). Taken alone, this evidence
6 indicates that either atmospheric forcing (via surface runoff) dominates oceanic
7 forcing (via SST), or *vice versa*. However, the occurrence of runs where α_3 does not
8 significantly exceed 0 (i.e. where runs experience negligible M variability)
9 demonstrate that the model can successfully reproduce observed behaviour with
10 nearly no changes in oceanic forcing from year to year. Although some successful
11 model runs did have significant inter-annual M variability (e.g. the maximum range of
12 M values for an entire 141 year model run was $0.76 \text{ km}^3 \text{ a}^{-1}$), each model run always
13 requires significant atmospheric forcing variability to allow it to replicate
14 observations. The importance of oceanic forcing variability can therefore not be
15 entirely discounted.

16 The model demonstrates that knowledge of atmospheric forcing **variability** (via
17 runoff), without needing to vary oceanic forcing, can be sufficient to reproduce
18 realistic patterns of observed glacier behaviour at KNS over the last century.
19 However, the precise physical mechanism by which air temperature could drive
20 observed change requires further investigation. For example, though a combination
21 of modelled and empirically estimated runoff values have been used to drive
22 changes in d_w to force the model, subglacial runoff variability is also known to drive
23 rates of submarine melting at the terminus (Jenkins, 2011; Xu et al., 2012; Sciascia
24 et al., 2013). Therefore we do not rule out that the behaviour observed could also be
25 explained by calving driven by seasonal changes in submarine melt rates, that are in
26 turn a function of subglacial runoff (e.g. Sciascia et al. 2013).

27 The relative insensitivity to changes in oceanic forcing is not necessarily
28 surprising given the hydrographic setting of KNS – located at the end of a >100 km
29 long fjord system that is thought to be largely insulated from changes in ocean
30 conditions due to the presence of a shallow sill at its entrance (Mortensen et al.,
31 2011; 2013). This has previously been used to suggest that recent changes in ocean
32 conditions (e.g. Straneo and Heimbach, 2013) have not affected the dynamics of
33 KNS significantly (Straneo et al., 2012). The results presented here are therefore
34 compatible with this argument.

1 The over-estimation of terminus retreat by 2012 of every successful run is
 2 thought to result from the poor knowledge of fjord width geometry beyond the
 3 contemporary glacier terminus. Upstream of the 2012 terminus, the lateral ice
 4 margins are used to define model glacier width, leading to a likely over-estimation of
 5 the prescribed fjord width. The divergence between the actual and prescribed fjord
 6 width is ~~therefore~~ likely to increase upglacier, increasing the likelihood of model error
 7 in this area. This explains why significant divergence from the observational record
 8 only occurs once the modelled terminus has retreated ~1.5 km beyond the 2012
 9 terminus (Figures 5a-c). Given the shallowing of the fjord bathymetry upstream of the
 10 2012 terminus (Figure 5c), fjord width uncertainty is likely to be the major cause of
 11 the model over-estimating retreat (Figure 5b). This also substantiates observations
 12 that destabilising changes in fjord width can dominate stabilising changes in fjord
 13 depth. However, ~~a~~Any attempt at modelling the future fluctuations of KNS will
 14 therefore require both improvements to subglacial topography estimates and
 15 comprehensive assessments of fjord width uncertainties as part of any predictions.

Formatted: Font: Not Italic

Formatted: Font: Not Italic

17 8. Conclusions

18 Utilising multiple lines of evidence, it has been possible to reconstruct terminus
 19 fluctuations of KNS from 1859-2012. This study therefore completes the record of
 20 terminus fluctuations of KNS from its LIAMax, in 1761 (Lea et al., 2014a), up to the
 21 present (~~Lea et al., 2014a~~), providing one of the longest, and most detailed records
 22 of observed TWG change in Greenland. The length and detail of this record, in
 23 conjunction with existing datasets providing boundary conditions, therefore make
 24 KNS an ideal validation site for models aiming to simulate outlet glacier retreat,
 25 and/or the impact of calving on tidewater glacier dynamics. At present the major
 26 boundary condition uncertainty is fjord topography, though what is known is sufficient
 27 for the model used in this study to replicate observed dynamics over multi-decadal to
 28 centennial timescales.

29 Results from numerical modelling show that the fluctuations of KNS can be
 30 simulated through parameterisations that link surface runoff to a crevasse water
 31 depth based calving criterion. Changes in ~~both/either~~ crevasse water depth and/or
 32 runoff driven rates of submarine melt are therefore suggested as potential drivers of
 33 observed change. Although ocean driven changes in submarine melt rates are not

Formatted: Indent: First line: 1.27 cm

1 always required for the model to replicate the observed length variations of KNS,
2 results do not allow their importance to be discounted entirely.

3 Observations of KNS show it to respond in phase with AT and SST anomalies
4 over multi-annual to decadal timescales from at least 1921-2012 (i.e. retreating
5 during positive temperature anomalies, and advancing during negative temperature
6 anomalies). However, where inter-annual comparisons to AT and SST are possible
7 (1992-2012), climatically anti-phased terminus fluctuations are observed. This
8 highlights the inherent noisiness of terminus response over short timescales, the
9 potential importance of antecedence, and the dangers of using similarly short
10 calibration periods for predictive modelling efforts.

11 Results from numerical modelling successfully capture the terminus dynamics
12 of KNS over multi-annual to decadal timescales, though not precise inter-annual
13 fluctuations. This is due to a combination of uncertainties in fjord topography, and the
14 approximations inherent to the depth and width integrations associated with using a
15 one-dimensional flow-band model.

16 Nevertheless, this study demonstrates that simple flow-band numerical
17 models of tidewater glaciers can be used to capture TWG dynamics over multi-
18 annual to centennial timescales. This provides validation that these models can be
19 useful tools for ~~both~~ palaeo, ~~and~~ contemporary, and prognostic modelling efforts.
20 However, the primary challenge to their use as predictive tools remains s the accurate
21 definition of subglacial topography and fjord width, which exert dominant controls on
22 ~~modelled~~ glacier stability. Any future efforts at prognostic modelling of TWGs should
23 therefore seek to account for these uncertainties in addition to those associated with
24 sensitivity to climate forcing.

25

26 **Acknowledgements**

27 The authors wish to thank Stephen Price, Mauri Peltó and an anonymous reviewer
28 for their reviews and comments that helped to improve the manuscript. RACMO2.1
29 data were provided by Jan van Angelen and Michiel van den Broeke, IMAU, Utrecht
30 University. MAR v3.2 data used for runoff calculations were provided by Xavier
31 Fettweis, Department of Geography, University of Liège. The photogrammetric DEM
32 used in Figures 1 and 3 was provided by Kurt H. Kjær, Centre for GeoGenetics,
33 University of Copenhagen. This research was financially supported by J.L.'s PhD
34 funding, NERC grant number: NE/I528742/1. Support for F.M.N. was provided by the

1 Conoco-Phillips/Lundin Northern Area Program CRIOS project (Calving Rates and
2 Impact on Sea Level).

3

4 **References**

5 Alley, R. B., Andrews, J. T., Brigham-Grette, J., Clarke, G. K. C., Cuffey, K. M.,
6 Fitzpatrick, J. J., and 7 others: History of the Greenland Ice Sheet: paleoclimatic
7 insights. *Quaternary Science Reviews*, 29(15), 1728-1756, 2010. DOI:
8 10.1016/j.quascirev.2010.02.007

9

10 Bamber, J. L., Layberry, R. L., Gogineni, S. P.: A new ice thickness and bed data set
11 for the Greenland ice sheet: 1. Measurement, data reduction, and errors. *Journal of*
12 *Geophysical Research: Atmospheres (1984–2012)*, 106(D24), 33773-33780, 2001.
13 DOI: 10.1029/2001JD900054

14

15 Bevan, S. L., Luckman, A. J., and Murray, T.: Glacier dynamics over the last quarter
16 of a century at Helheim, Kangerdlugssuaq and 14 other major Greenland outlet
17 glaciers, *The Cryosphere*, 6, 923-937. DOI:10.5194/tc-6-923-2012, 2012.

18

19 Brede, N.: *Skizze Kaart over Vestkysten af Grønland fra Arsuk til Holsteensborg*.
20 KBK Netpublikation DK003200, Copenhagen, 1866.

21

22 Bjørk, A. A., Kjær, K. H., Korsgaard, N. J., Khan, S. A., Kjeldsen, K. K., Andresen, C.
23 S., Larsen, N.K., Funder, S.: An aerial view of 80 years of climate-related glacier
24 fluctuations in southeast Greenland. *Nature Geoscience*, 5(6), 427-432, 2012. DOI:
25 10.1038/ngeo1481

26

27 Bruun, D.: Oversigt over Norburuiner i Godthaab og Frederikshaab Distrikter.
28 *Meddelelser om Grønland*. 56(3), 55-147, 1917.

29

30 Cappelen, J.: Greenland-DMI Historical Climate Data Collection 1873-
31 2011. *Technical Report 12-04*. Copenhagen, 2012. ISSN: 1399-1388

32

- 1 Colgan, W., Pfeffer, W. T., Rajaram, H., Abdalati, W.: Monte Carlo ice flow modeling
2 projects a new stable configuration for Columbia Glacier, Alaska, by c.
3 2020. *Cryosphere*, 6(2), 893-930, 2012. DOI: 10.5194/tcd-6-893-2012
4
- 5 Cook, S., Zwinger, T., Rutt, I. C., O'Neel, S., Murray, T.: Testing the effect of water in
6 crevasses on a physically based calving model. *Annals of Glaciology*, 53(60), 90-96,
7 2012. DOI: 10.3189/2012AoG60A107
8
- 9 Cook, S., Rutt, I. C., Murray, T., Luckman, A., Selmes, N., Goldsack, A., Zwinger, T.:
10 Modelling environmental influences on calving at Helheim Glacier, East
11 Greenland. *Cryosphere Discussions*, 7(5), 2013. DOI: 10.5194/tcd-7-4407-2013
12
- 13 Csatho, B., Schenk, T., Van der Veen, C. J., Krabill, W. B.: Intermittent thinning of
14 Jakobshavn Isbræ, West Greenland, since the Little Ice Age. *Journal of*
15 *Glaciology*, 54(184), 131-144, 2008. DOI: 10.3189/002214308784409035
16
- 17 Rink, H.: *Kyststrækning fra Frederikshåb i syd til Napasaq i nord*. KBK Netpublikation
18 RI000029, Copenhagen, 1866.
19
- 20 Fettweis, X., Tedesco, M., Broeke, M., Ettema, J.: Melting trends over the Greenland
21 ice sheet (1958–2009) from spaceborne microwave data and regional climate
22 models. *The Cryosphere*, 5(2), 359-375, 2011. DOI: 10.5194/tc-5-359-2011
23
- 24 Gogineni, S., Tammana, D., Braaten, D., Leuschen, C., Akins, T., Legarsky, J. and 4
25 others, K.: Coherent radar ice thickness measurements over the Greenland ice
26 sheet. *Journal of Geophysical Research: Atmospheres (1984–2012)*, 106(D24),
27 33761-33772, 2001. DOI: 10.1029/2001JD900183
28
- 29 Hanna, E., Cappelen, J., Fettweis, X., Huybrechts, P., Luckman, A., Ribergaard, M.
30 H.: Hydrologic response of the Greenland ice sheet: the role of oceanographic
31 warming. *Hydrological Processes*, 23(1), 7-30, 2009. DOI: 10.1002/hyp.7090
32

- 1 Howat, I. M., Eddy, A.: Multi-decadal retreat of Greenland's marine-terminating
2 glaciers. *Journal of Glaciology*, 57(203), 389-396, 2011. DOI:
3 10.3189/002214311796905631
4
- 5 Hvidegaard, S.M., Sorensen, L.S., Forsberg, R.: ASTER GDEM validation using
6 LiDAR data over coastal regions of Greenland. *Remote Sensing Letters*, 3(1), 85–
7 91, 2012. DOI: 10.1080/01431161.2010.527389
8
9
- 10 Jamieson, S. S., Vieli, A., Livingstone, S. J., Cofaigh, C. Ó., Stokes, C., Hillenbrand,
11 C. D., Dowdeswell, J. A.: Ice-stream stability on a reverse bed slope. *Nature*
12 *Geoscience*, 5(11), 799-802, 2012. DOI: 10.1038/ngeo1600
13
- 14 Jamieson, S. S. R., A. Vieli, C. Ó Cofaigh, C. R. Stokes, S. J. Livingstone, and C.-D.
15 Hillenbrand: Understanding controls on rapid ice-stream retreat during the last
16 deglaciation of Marguerite Bay, Antarctica, using a numerical model, *Journal of*
17 *Geophysical Research: Earth Surface*, 119, 247–263, 2014.
18 DOI:10.1002/2013JF002934.
19
- 20 Jenkins, A.: Convection-Driven Melting near the Grounding Lines of Ice Shelves and
21 Tidewater Glaciers. *Journal of Physical Oceanography*, 41(12), 2011. DOI: .
22
- 23 Jensen, J.A.D.: *Vestkysten af Grönland fra Arsuk til Holstensborg 61° til 67° N*. KBK
24 Netpublikation, DK003198. Copenhagen, 1885
25
- 26 Joughin, I., Smith, B. E., Howat, I. M., Scambos, T., Moon, T.: Greenland flow
27 variability from ice-sheet-wide velocity mapping. *Journal of Glaciology*, 56(197), 415-
28 430, 2010. DOI: 10.3189/002214310792447734
29
- 30 Kleinschmidt, S.: *Godthåbs distrikt (hertil en Navneliste)*. (Map No. KBK
31 Netpublikation RI000074). Copenhagen, 1859.
32
- 33 Lea J.M., Mair, D.W.F., Nick, F.M., Rea., B.R., Weidick, A., Kjær, K., Morlighem, M.,
34 van As, D., Schofield, J.E.: Terminus-driven retreat of a major southwest Greenland

1 Xu, Y., Rignot, E., Menemenlis, D., Koppes, M.: Numerical experiments on
2 subaqueous melting of Greenland tidewater glaciers in response to ocean warming
3 and enhanced subglacial discharge. *Annals of Glaciology*, 53(60), 229-234, 2012.
4 DOI: 10.3189/2012AoG60A139

5

6

7

8

1 Table 1. List of terminus observations and acquisition dates.

<i>Acquisition</i>		
<i>date</i>	<i>Observation type</i>	<i>Source</i>
1850s	Terrestrial photo'	H. Rink (in Weidick et al, 2012)
1859	Map	Kleinschmidt (1859)
1860	Map	Poulsen (1860)
1866	Map	Rink (1866)
1866	Map	Falbe (1866)
1885	Map	Jensen (1885)
1880s?	Sketch (after photo')	Nansen (1890)
1903	Terrestrial photo'	J. Møller in Bruun (1917)
1921	Terrestrial photo'	A. Nissen in Weidick et al (2012)
1932	Terrestrial photo'	A. Roussell in Roussell (1941)
27/08/1936	Oblique photo'	Weidick et al (2012)
10/08/1946	Oblique photo'	Weidick et al (2012)
20/08/1948	Oblique photo'	Weidick et al (2012)
21/06/1965	Terrestrial photo'	Weidick et al (2012)
16/08/1968	Aerial photo'	USGS
15/09/1979	Terrestrial photo'	Weidick et al (2012)
15/09/1987	Satellite	Landsat
19/09/1992	Satellite	Landsat
30/08/1993	Satellite	Landsat
18/09/1994	Satellite	Landsat
14/10/1995	Satellite	Landsat
14/09/1996	Satellite	Landsat
01/09/1997	Satellite	Landsat
15/09/1999	Satellite	Landsat
18/09/2000	Satellite	Landsat
22/10/2001	Satellite	Landsat
23/09/2002	Satellite	Landsat
09/08/2003	Satellite	Landsat

12/09/2004	Satellite	Landsat
24/09/2005	Satellite	Landsat
18/09/2006	Satellite	Landsat
27/09/2007	Satellite	Landsat
23/09/2008	Satellite	Landsat
19/09/2009	Satellite	Landsat
13/09/2010	Satellite	Landsat
16/09/2011	Satellite	Landsat
18/09/2012	Satellite	Landsat

1

2

3

1 Table 2. List of parameters and constants used for running the model

<i>Parameter/Constant</i>	<i>Value</i>
Ice density – ρ_i	900 kg m ⁻³
Meltwater density – ρ_w	1000 kg m ⁻³
Proglacial water body density – ρ_p	1028 kg m ⁻³
Gravitational acceleration - g	9.8 m s ⁻²
Friction exponent - m	3
Friction parameters – μ and λ	1
Glen's flow law exponent - n	3
Glen's flow law coefficient - A	4.5 x 10 ⁻¹⁷ Pa ⁻³ a ⁻¹ (-5°C)
Grid size	~250 m
Time step	0.005 a

Formatted: Not Superscript/ Subscript

2

3

4

1 Table 3. Pearson correlation coefficient values for tuning parameters of successful
 2 model runs ($n = 29$). Correlation coefficients with p-values < 0.05 are highlighted in
 3 bold.

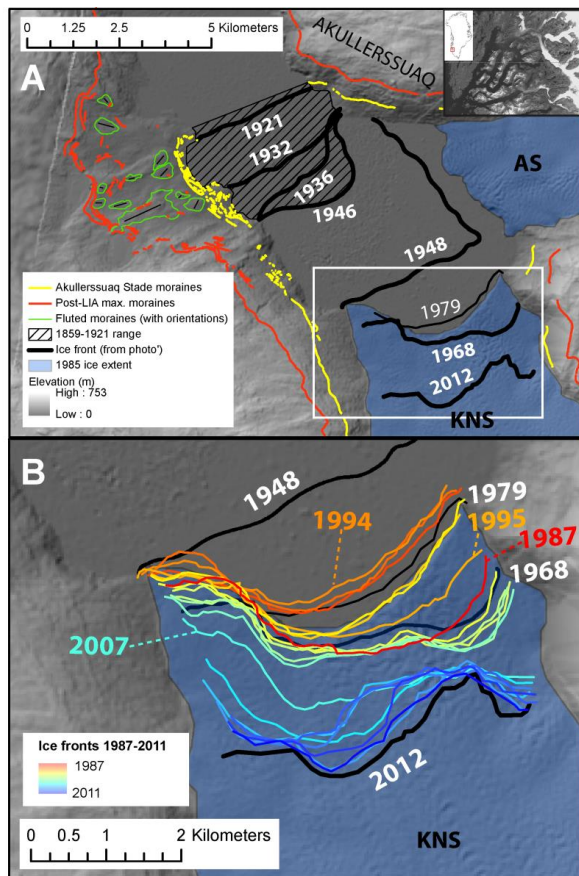
	α_1	α_2	α_3	<i>Mbase</i>
α_1	-	-0.92285	0.287883	-0.46884
α_2	-0.92285	-	-0.46065	0.292157
α_3	0.287883	-0.46065	-	-0.42711
<i>Mbase</i>	-0.46884	0.292157	-0.42711	-

4

5

6

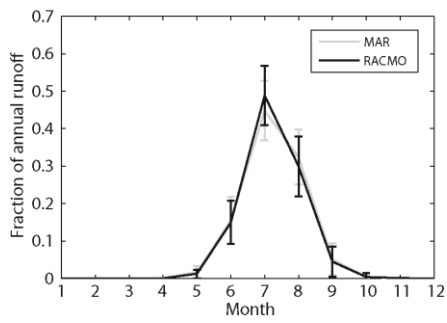
7



1
 2 Figure 1. Diagrams showing the site location (inset), terminus positions and
 3 geomorphology plotted on a hillshaded mosaic of a stereophotogrammetrically
 4 derived digital elevation model (DEM) from images acquired in 1985, and ASTER
 5 GDEM (Hvidegaard et al., 2012). (A) termini and geomorphology for 1859-2012, with
 6 ASM limits delineated in yellow, and (B) a detailed view of termini for the period
 7 1948-2012, with specific years labelled for reference.

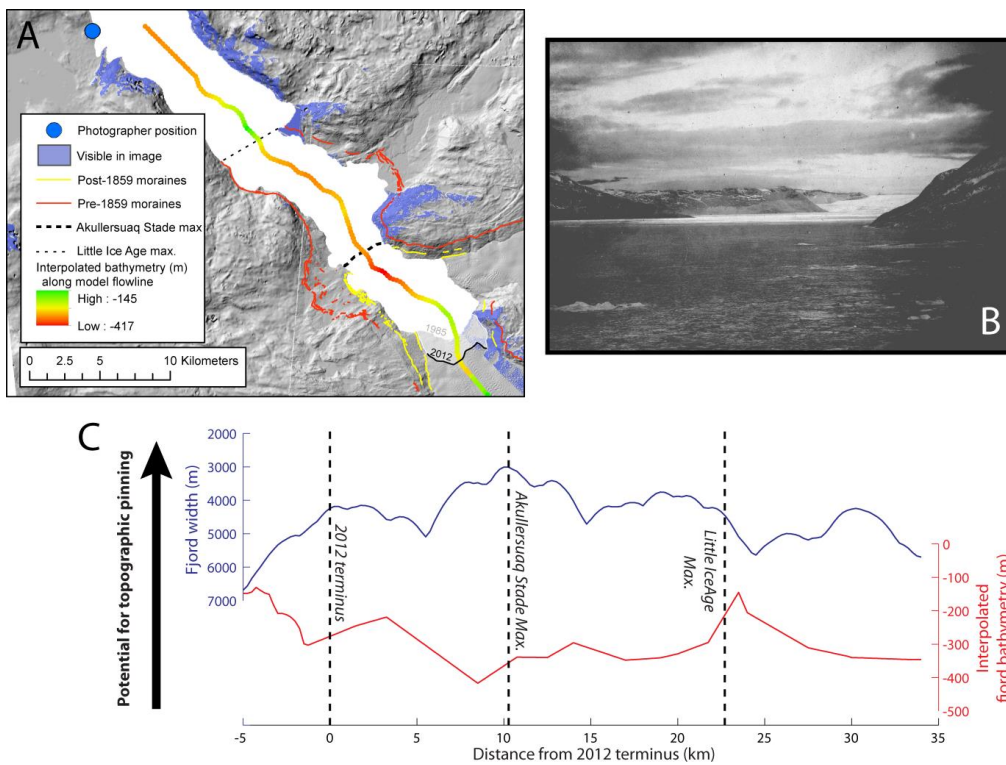
8

9



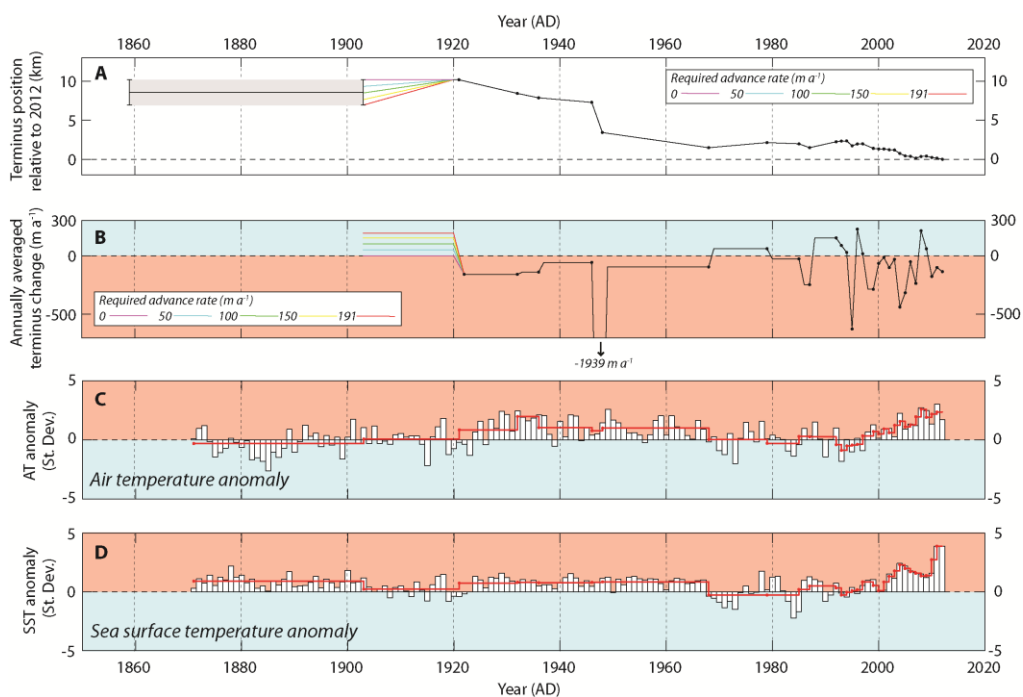
1
2 Figure 2. Fraction of annual runoff occurring for each month as given by MAR and
3 RACMO2 SMB models for KNS and AS between 1960-2012 (Van As et al., in
4 press). Error bars are given to 2 standard deviations.

5
6
7

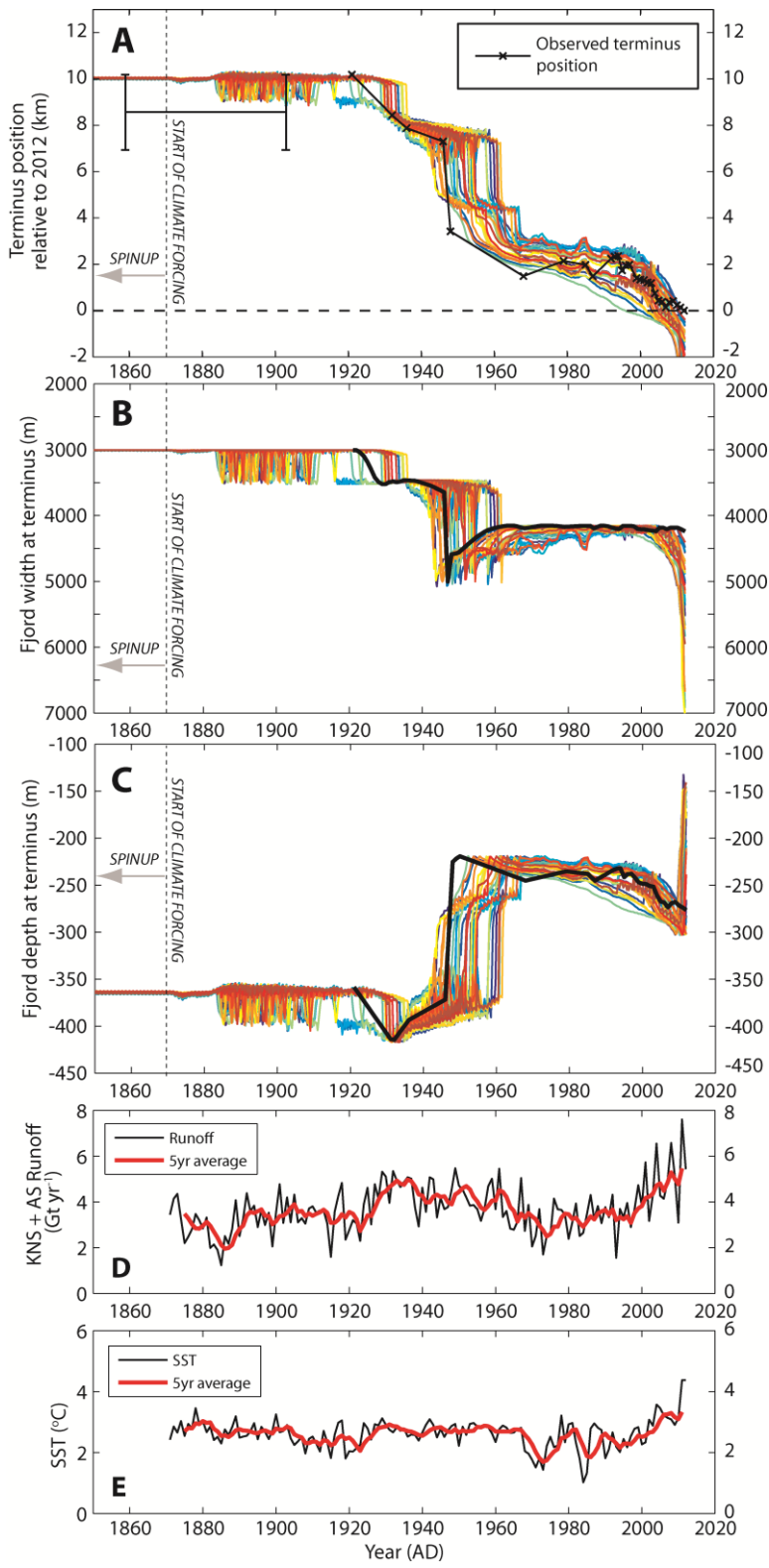


1
 2 Figure 3. Viewshed analysis. (A) 1985 hillshaded DEM (see Figure 1), with
 3 reconstructed photographer position showing areas that would be observable in the
 4 photograph, and the path of the model flowline colour-coded for showing
 5 the interpolated fjord bathymetry, (B) the photograph of KNS acquired in 1903, (C)
 6 along-fjord width and depth relative to the 2012 terminus position. Note that fjord
 7 width is plotted on a reversed axis to reflect the relative potential for the occurrence
 8 of topographic pinning points.

9
 10
 11

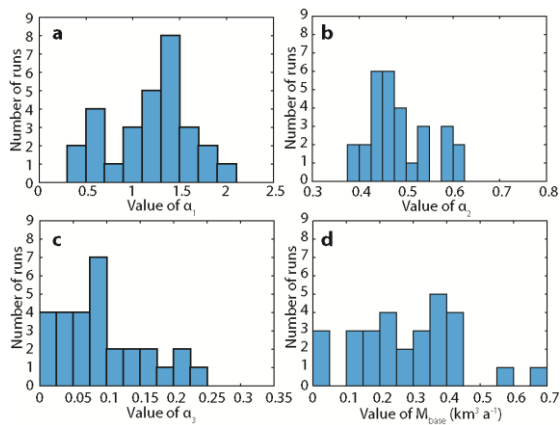


1
 2 Figure 4. (A) Terminology position relative to the 2012 terminus position. Uncertainty in
 3 terminus position for 1859-1903 highlighted in grey, with a range of potential
 4 advance rates for 1903-1920 indicated. These range from a minimum of no change
 5 ($0 m a^{-1}$) to a maximum possible advance rate of $191 m a^{-1}$. (B) Annually averaged
 6 rates of terminus change between observations (black dots). Includes terminus
 7 advance rates described for 1903-1921 terminus change indicated on A. (C)
 8 Summer ATA (June, July, August) at annual resolution (white bars), and red line
 9 showing the averaged ATA between terminus observations (Cappelen et al, 2012;
 10 Vinther et al, 2006). (D) Annual SSTA for the area 61° to 65° N 51° to 56° W at
 11 annual resolution (white bars) and red line showing the averaged SSTA between
 12 terminus observations (Rayner et al, 2003).
 13



1 Figure 5. (A) Evolution of terminus position for model runs (coloured lines)
 2 determined to be successful according to the criteria outlined in the text, with
 3 observed terminus position also plotted (bold black line, with positions between
 4 observations linearly interpolated). (B) Evolution of fjord width at the terminus, with
 5 values interpolated from observations plotted in black, (C) Evolution of fjord depth at
 6 the terminus, with values interpolated from observations plotted in black, (D)
 7 Combined KNS and AS runoff volume estimates for 1871-2012 that are used to
 8 drive the model (5 year moving average also plotted in red). (E) Absolute annual
 9 SST estimates used to drive the model from Rayner et al. (2003) for the area 61° to
 10 65° N and 51° to 56° W (5 year moving average also plotted in red).

11



12

13 Figure 6. The distribution of the tuning parameters (a) α_1 (bin width = 0.2), (b)
 14 α_2 (bin width = 0.025), (c) α_3 (bin width = 0.025), and (d) M_{base} (bin width = 0.05 $\text{km}^3 \text{a}^{-1}$) for
 15 successful runs as defined by the criteria outlined in the text. Minimum and
 16 maximum x-axis values represent the full range of values tested within the 1500
 17 model runs.